Applied Catalysis B: Environmental 117–118 (2012) 67–72

Contents lists available at SciVerse ScienceDirect

Applied Catalysis B: Environmental

journal homepage: www.elsevier.com/locate/apcatb

Mesoporous PdO–TiO_2 nanocomposites with enhanced photocatalytic activity

Adel A. Ismail[a,b,*]

[a] Nanostructured & Nanotechnology Materials Division, Advanced Materials Department, Central Metallurgical R&D Institute, CMRDI, P.O. Box 87, Helwan 11421, Cairo, Egypt
[b] Centre for Advanced Materials and Nanoengineering (CAMNE), Najran University, P.O. Box 1988, Najran 11001, Saudi Arabia

ARTICLE INFO

Article history:
Received 30 October 2011
Received in revised form
20 December 2011
Accepted 3 January 2012
Available online 9 January 2012

Keywords:
Mesoporous
PdO–TiO_2
Nanocomposites
Photocatalytic
Oxidation
Methanol

ABSTRACT

Herein, we report a synthesis of mesoporous PdO–TiO_2 nanocomposites at different PdO (0–3 wt%) through simple one-step sol–gel reactions. Pd^{2+} ions have been immobilized into TiO_2 networks by cross-linking triblock copolymer (Pluronic F123) as the structure-directing agents to develop highly efficient PdO–TiO_2 photocatalyst. The produced PdO–TiO_2 gel were calcined at 400 °C for 4 h to remove organic materials. TiO_2 nanoparticles with an average diameter are 8–10 nm and PdO nanoparticles are well dispersed and exhibit diameters of about 10–40 nm based on the PdO content. Our prepared photocatalysts have been compared with Pd/Aeroxide TiO_2-P25 by the determination of the initial rate of HCHO formation generated by the photooxidation of CH_3OH in aqueous suspensions to calculate the corresponding photonic efficiencies. The newly prepared PdO–TiO_2 nanocomposites showed a more effective and high efficient photocatalytic activities for CH_3OH oxidation to HCHO ~4 and 2 times than TiO_2-P25 and Pd/TiO_2-P25 respectively. In the present work, the photocatalytic activities of the obtained PdO–TiO_2 nanocomposites were significantly higher than those of previously reported. To the best of our knowledge, the measured photonic efficiency ξ = 19.5% of mesosporous PdO–TiO_2 nanocomposites is found to be among the highest ξ-values reported up to now.

1. Introduction

Mesoporous materials have attracted considerable interest for their applications as catalysts, gas separators, sensors, and energy converters [1–3]. TiO_2 mesoporous is an interesting material for photocatalytic applications due it is continuous, which may be beneficial compared to separated individual nanoparticles, in particular for catalyst recovery [1–4]. Two of the most important factors affecting the photocatalytic activity of TiO_2 are its specific surface area in a continuous structure rather than in discrete particles and crystallinity. This continuity can be expected to make the electron transfer within the material easier, resulting in higher activity [4]. If mesoporous TiO_2 could be prepared with an anatase crystalline wall, it would be a useful material applicable to high performance photocatalyst. In the last decade, research efforts have been directed to enhance the activity of the mesoporous TiO_2 photocatalysts using various methods such as increasing catalyst surface-to-volume ratio, sensitization of the catalyst using dye molecules [5,6], doping the catalyst with nonmetals such as nitrogen, carbon, fluoride and iodine [7–10] and transition metals [10–13]. Also, loading of noble metals with mesoporous TiO_2 photocatalysts was proposed to enhance the photocatalytic activity due to their different Fermi levels, characterized by the work function of the metals and the band structure of the semiconductors. Upon contact, a Schottky barrier can be formed between the TiO_2 and the noble metals, leading to a rectified charge carrier transfer [14–18]. An increase in the photocatalytic activity when a certain metal is deposited is generally explained by attraction of electrons to the metal particles on TiO_2 followed by reduction in the recombination rate of electrons with holes [14–18]. Although Pt-based catalysts have superb activity and performance for oxygen reduction, Pt may ultimately not be practical for large-scale commercialization of catalysts due to its limited supply and high cost. As one of the alternative catalysts, Pd was found to be an acceptable alternative to Pt for catalysts [19,20]. It is known that the photocatalytic process mainly takes place on the surface of catalysts and involves comprehensive competing reactions. Therefore, the surface properties of TiO_2, such as surface acidity, defects, and hydroxyl groups, can greatly affect the reaction efficiency [21]. Among them, hydroxyl groups can give rise to a great influence on the chemical properties of TiO_2 [22–24]. The importance of surface hydroxyl groups is related to two aspects: scavenging of holes and adsorption centers for reactants and intermediates [25]. Moreover, the oxidation reaction of CH_3OH in our experiment was believed to be initiated by •OH radicals [26]. We have employed methanol to determine the amount of •OH radicals produced in the photocatalytic process. The measurement of the rate of •OH radical

* Correspondence address: Nanostructured & Nanotechnology Materials Division, Advanced Materials Department, Central Metallurgical R&D Institute, CMRDI, P.O. Box 87, Helwan 11421, Cairo, Egypt.

0926-3373/$ – see front matter © 2012 Elsevier B.V. All rights reserved.
doi:10.1016/j.apcatb.2012.01.006

generation is one of the most important parameters to be studied during the evaluation of newly developed photocatalysts [14–18].

In our previous published work [14], we have reduced Pd^{2+} directly using H_2 gas and its photonic efficiency was $\xi = 16.3\%$ for CH_3OH photooxidation. Therefore, synthesis of small Pd nanoparticles and TiO_2 porous nanostructures with interconnected structures can combine both assets in enhancing the photocatalytic activities as they can supply different adsorption sites for the reactions involving two or more reactants. Li et al. [27] have succeeded to syntheses gold nanoparticles within the titania framework, titania, and gold building clusters were cooperatively assembled in an one-step process. They have used Pluronic surfactant P123, $TiCl_4$, $Ti(OBu)_4$, and $AuCl_3$ were mixed in ethanol. These unique mesoporous Au/TiO_2 nanocomposites with different Au loadings show significantly improved photocatalytic activities for phenol oxidation and chromium reduction. From this window, we have completely changed the preparation method as shown in Ref. [14] to enhance the photonic efficiency. In the present work, $PdO–TiO_2$ nanocomposites synthesized from TBOT and $TiCl_4$ with Pd(II) as the inorganic precursors and the triblock copolymer $EO_{20}PO_{70}–EO_{20}$ (F123) as the template were achieved by a simple one-step. Pd^{2+} ions have been reduced to Pd^0 during the initial state of the photocatalytic oxidation of CH_3OH, photogenerated electrons were transferred from TiO_2 conduction band to the Pd^{2+} ions and simultaneously CH_3OH was oxidized to HCHO. Interestingly, in this work, the measured photonic efficiency is found to be $\xi = 19.5\%$ of mesosporous 0.5% $PdO–TiO_2$ nanocomposites.

2. Experimental

2.1. Materials

Pluronic P123 (a poly (ethylene oxide)-poly (propylene oxide)-poly (ethylene oxide) block copolymer $EO_{20}PO_{70}–EO_{20}$, Aldrich) served as a structure-directing agent. $TiCl_4$, $Ti(OC(CH_3)_3)_4$ (TBOT), HCl, CH_3OH, C_2H_5OH, and $PdCl_2$ were purchased from Sigma–Aldrich.

2.1.1. Preparation of $PdO–TiO_2$ nanocomposites

Highly ordered $PdO–TiO_2$ nanocrystals were synthesized through a simple one-step sol–gel process in the presence of the P123 triblock copolymer as structure directing agent. To homogenously embed PdO nanoparticles within the titania framework, we utilized a multicomponent assembly approach, where surfactant, TiO_2, and PdO building clusters were cooperatively assembled in an one-step process. In a typical synthesis, transparent sols were prepared by mixing 1.0 g P123, 1.7 g $TiCl_4$, 3.0 g $Ti(OBu)_4$, certain amount of $PdCl_2$ with 20.0 mL ethanol at room temperature and casting the sols in Petri dish to form a thin gel layer. After aging at 40 °C for 24 h and 100 °C for 12 h, the gels were calcined at 400 °C for 4 h in air using a heating rate of 0.5 °C/min. Calcination removed P123 and created crystalline mesoporous TiO_2 networks embedding PdO nanoparticles.

2.1.2. Preparation of Pd/commercial Aeroxide TiO_2-P25 (Evonik AG)

Pd was photochemically deposited onto commercial Aeroxide TiO_2-P25 as follows: 0.5 g of Aeroxide TiO_2-P25 was suspended by stirring in 100 mL aqueous methanol solution (1.0 v.%) containing specific concentration of $PdCl_2$ to obtain varied 0.5% Pd/TiO_2-P25. The resulting solution was irradiated with UV(A) light by a Philips Hg lamp (illumination intensity at 350 nm: 1.0 mW cm^{-2}) for 12 h. The obtained powder was separated by centrifugation, washed with water and dried at 110 °C for 12 h.

2.2. Characterization

Transmission electron microscopy (TEM) was conducted at 200 kV with a JEOL JEM-2100F-UHR field-emission instrument equipped with a Gatan GIF 2001 energy filter and a 1k-CCD camera in order to obtain EEL spectra. Wide angle X-ray diffraction (WXRD) data were acquired on a Bruker AXS D4 Endeavour X diffractometer using Cu $K\alpha_{1/2}$, $\lambda\alpha_1 = 154.060$ pm, $\lambda\alpha_2 = 154.439$ pm radiation and small angle X-ray diffraction (SXRD) patterns were recorded on a Bruker D8 advance. The nitrogen adsorption and desorption isotherms at 77 K were measured using a Quantachrome Autosorb 3B after the samples were vacuum-dried at 200 °C overnight. The sorption data were analyzed using the Barrett–Joyner–Halenda (BJH) model with Halsey equation [28].

2.3. Photocatalytic activity tests

The quartz photoreactor was filled with 75 mL aqueous solution of methanol at a concentration 30 mM. UV irradiation was performed by a 450 W medium pressure xenon lamp (Osram) placed inside a quartz jacket and equipped with a cooling tube. The lamp was switched on 30 min prior to the start of the reaction to stabilize the power of its emission at $\lambda > 320$ nm (a cut-off filter was used to remove light with wavelengths below 320 nm) and the reactor was cooled by circulation of H_2O. The temperature of the cooling water was stabilized to perform the reactions at 25 °C. Photooxidation reactions were carried out suspending 0.5 g/L of either mesoporous $PdO–TiO_2$ with oxygen being purged through the reaction vessel continuously. The suspensions were sonicated at the desired aqueous solution of methanol [30 mM] before the experiment was started and they were stirred in the dark for 30 min to reach the adsorption equilibrium prior to irradiation. HCHO samples were withdrawn at regular intervals from the upper part of the reactor with the catalyst being removed from the liquid phase by filtration through nylon syringe filters (pore size: 0.45 μm). The photooxidation rate was determined by measuring the HCHO generated as a result of methanol oxidation during the first 60 min of illumination employing the Nash method [29]. The detection limit for HCHO determined by the Nash method is 1.66 μM. The relative error of the measured HCHO concentration was ±5% as judged from repeated runs under identical conditions. This method is based on the reaction of formaldehyde with acetylacetone and ammonium acetate to form a yellow colored product with a maximum of absorbance at 412 nm. Measurements were carried out using a Varian Cary 100 Scan UV–vis spectrophotometer, following an incubation time of 15 min at 60 °C. The photonic efficiency was calculated for each experiment as the ratio of the HCHO formation rate and the incident light intensity as given in the following equation [30].

$$\xi = \frac{r \times 100}{I}$$

where ξ is the photonic efficiency (%), r is the photooxidation rate of methanol (mol L^{-1} s^{-1}), and I is incident photon flux. The incident photon flux in the wavelength range $300\ \text{nm} \le I \le 400\ \text{nm}$ was determined by ferrioxalate actinometry [31] to be 4.94×10^{-6} Einstein L^{-1} s^{-1}. The lamp was switched on 30 min before the beginning of the reaction to stabilize the power of its emission spectrum. The actinometry was performed in the same photochemical reactor with the same volume of actinometric solution as the photocatalytic test, eliminating the errors associated with the influence of light reflections and reactor geometry. A 10 cm water bath and a black cut-off filter (3 mm, UG1 SCHOTT glass) were used during photon flux and photonic efficiency measurements.

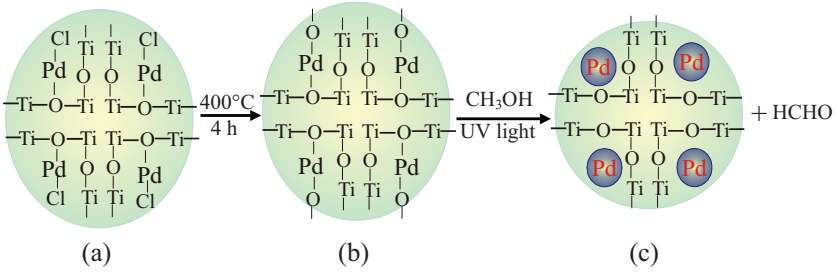

Scheme 1. Schematic illustration of the formation of mesoporous PdO–TiO_2 nanocomposites (a) before calcination and (b) after calcination and Pd/TiO_2 with embedded Pd nanoparticles after photooxidation of methanol to formaldehyde (c).

3. Results and discussion

PdO–TiO_2 nanocomposites synthesized from TBOT and $TiCl_4$ with Pd(II) as the inorganic precursors and the triblock copolymer $EO_{20}PO_{70}$–EO_{20} (F123) as the template were achieved by a simple one-step. These nanoparticles are quite stable and grow slowly to get transparent gel. An additional aging step is therefore required to condense the frameworks. After the organic solvents have been removed from the inorganic framework through drying at 65 °C, an amorphous inorganic solid with ordered mesopores has been produced. Subsequent heat-treatment at 400 °C has been forced desirable PdO–TiO_2 nanocomposites to nucleate and grow from the nanocrystalline matrix (see Scheme 1). Wide angle X-ray scattering (WAXS) patterns of highly ordered mesoporous PdO–TiO_2 at different PdO contents calcined at 400 °C for 4 h are shown in Fig. 1. Calcination at 400 °C led to initiate crystallization and appear of the (1 0 1), (0 0 4), (2 0 0) and (2 1 1) anatase peaks. No crystalline phase involving PdO can be observed, suggesting that either PdO may be incorporated into TiO_2 network or that the PdO content is below the detection limit. Small angle X-ray scattering (SAXS) patterns of highly ordered mesoporous as-made 1 wt% PdO–TiO_2 and mesoporous PdO–TiO_2 calcined at 400 °C for 4 h before and after photocatalytic reactions are shown in Fig. 2. The as-made sample show one well-resolved peak with a shoulder, which can be indexed as the (1 0 0) and (2 0 0) reflections of a two-dimensional hexagonal phase confirming an ordered mesostructure of *P6mm* space group [19]. Both samples have several well-resolved peak, these peaks can be indexed to (1 0 0) Bragg reflections confirming an ordered 2D-hexagonal mesostructure of *P6mm* space group. However, the structural regularity declined slightly and the d_{100} value decreased due to structural shrinkage as a result of calcinations at 400 °C. The shrinkage of the mesostructure is related to the elimination of the copolymer template and the formation of nanocrystalline anatase in the frameworks during the thermal treatment process. The unit cell parameter calculated from SAXS analysis is 14.01 and 12.11 nm for as-synthesized and calcined samples, respectively. Also, the findings of mesoporous PdO–TiO_2 calcined at 400 °C for 4 h before and after photocatalytic reactions confirmed that the incorporation of PdO nanoparticles into the TiO_2 framework does not completely destroy the latter's mesostructure even after the photocatalytic reactions.

Fig. 3 shows nitrogen adsorption–desorption isotherms and Barrett–Joyner–Halenda (BJH) pore-size distribution plots of the mesoporous PdO–TiO_2 nanocomposites at different PdO contents. The samples show similar type-IV isotherms, which are representative of mesoporous solids [32]. The sharpness of the inflection resulting from capillary condensation at relative pressures p/p_0 between 0.45 and 0.8 is characteristic for mesopores in 2D-hexagonal symmetry. The mesoporous TiO_2 has high surface areas of 183 $m^2\ g^{-1}$ and large pore volumes of 0.3 $cm^3\ g^{-1}$; they are gradually reduced to 103 $m^2\ g^{-1}$ and 0.22 $cm^3\ g^{-1}$, respectively, as a result of the PdO addition (Table 1). The slight decrease in pore size with the PdO addition at low content reveals that the thickness of the pore walls increases concomitantly from 6.66 to 6.77 nm, which is typical for surfactant templated mesoporous materials. Compared with the size of the TiO_2 nanocrystallites between 10 ± 2 nm (Table 1), the wall thickness is found to be slightly smaller, implying that some of the TiO_2 nanocrystals could partially pierce even into the channel space [33], which is particularly evident from the HRTEM images (Fig. 4e and f).

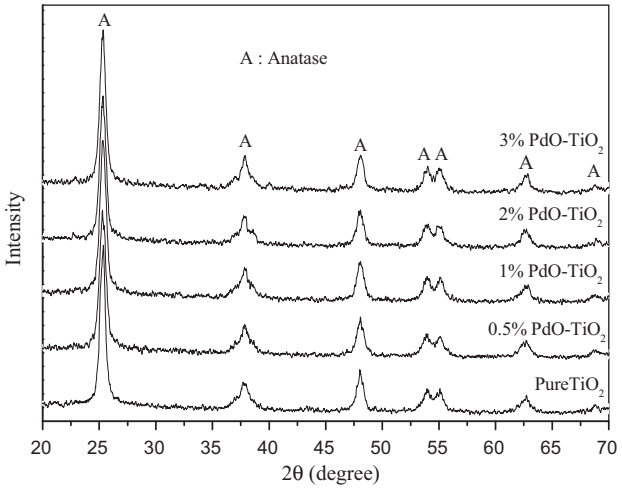

Fig. 1. WXRD of mesoporous PdO–TiO_2 nanocomposites calcined at 400 °C at different PdO wt% 0 (a), 0.5 (b), 1 (c), 2 (d) and 3 (e). Shifted for sake of clarity.

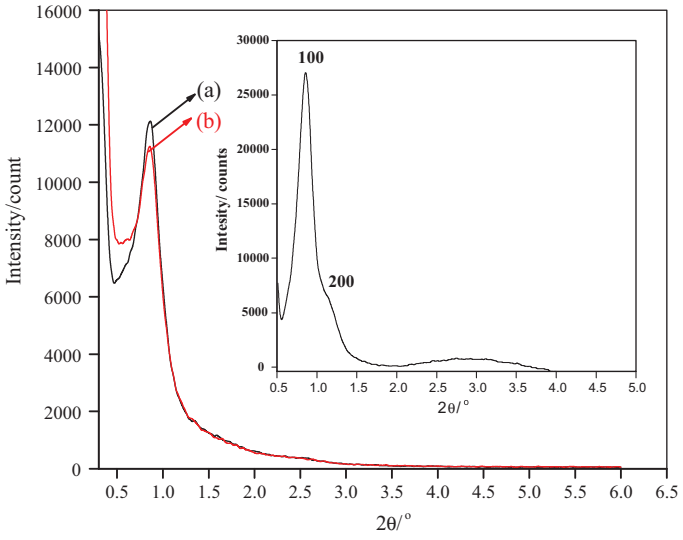

Fig. 2. SAXS patterns of as made 1 wt% PdO–TiO_2 (inset) and 1 wt% PdO–TiO_2 nanocomposites calcined at 400 °C before (a) and after (b) photocatalytic reactions.

Table 1
Textural properties of mesoporous PdO–TiO_2 nanocomposites at different PdO contents calcined at 400 °C and TiO_2-P25 and Pd/TiO_2-P25 and their photonic efficiencies.

Photo-catalysts	S_{BET} ($m^2\ g^{-1}$)	Pd particle size (nm)	$r \times 10^7$ ($mol\ L^{-1}\ s^{-1}$)	ξ (%)	d_{100} (nm)	Unit cell size (nm)	Pore wall (nm)	V_p ($cm^3\ g^{-1}$)	D_p (nm)
Meso-TiO_2	183	–	3.90	7.90	12.96	13.34	6.66	0.32	6.68
0.5% PdO–TiO_2	162	10	9.68	19.6	11.39	12.33	6.68	0.29	6.65
1% PdO–TiO_2	147	15	7.60	15.4	11.24	12.66	6.86	0.27	6.56
2% PdO–TiO_2	125	20	6.66	13.5	11.22	12.35	7.15	0.23	6.35
3% PdO–TiO_2	103	35	5.23	10.6	11.38	12.11	6.77	0.22	6.31
TiO_2-P25	45	–	2.02	4.10	–	–	–	–	–
0.5% Pd/TiO_2-P25	34	–	5.16	10.5	–	–	–	–	–

S_{BET} surface area; r, HCHO formation rate; ξ, photonic efficiency; V_p, pore volume; D_p, pore diameter.

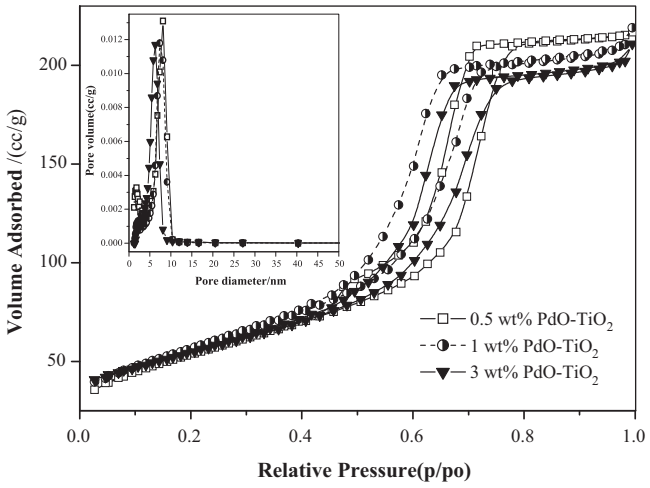

Fig. 3. N_2 sorption isotherms and pore size distributions (inset) of the mesoporous of PdO/TiO_2 nanocomposites calcined at 400 °C at different 0.5, 1 and 3 wt% PdO.

TEM images of mesoporous PdO–TiO_2 nanocomposites calcined at 400 °C for 4 h are presented in Fig. 4. The TEM images (Fig. 4a and b) of the mesoporous 0.5 and 1 wt% PdO–TiO_2 nanocomposites show a well-defined 2D hexagonal mesostructure, evincing the formation of a highly ordered mesostructure, which is consistent with the analysis of the SAXS pattern. The selected area electron diffraction (SAED) patterns (Fig. 4b inset) further confirm that anatase nanocrystallites are indeed formed. The particle size of these TiO_2 nanocrystals has been measured to be between 8 and 10 nm. The PdO nanoparticles are found to be much larger than the TiO_2 nanocrystals. HE-TEM image showed that both sorts of nanoparticles, TiO_2 and PdO, are partly in close contact as seen most impressively in Fig. 4d. Both, the HRTEM image (Fig. 4d) and the selective area electron diffraction (SAED, inset Fig. 4b) show well resolved (1 0 1) lattice fringes (distance: 0.352 nm) and diffraction cycles indicative of crystalline TiO_2 anatase. The PdO nanoparticles can be more easily found in bright and dark field TEM (BF-TEM) images (Fig. 3c, e and f) showing that PdO nanoparticles are well dispersed and the average PdO particle diameters increase from ~10 nm in the 0.5 wt% PdO–TiO_2 sample to 35 nm for the samples with high 3 wt% PdO content. Energy dispersive X-ray spectra (EDXS) also reveal the presence of Pd^{2+} and confirm that the final

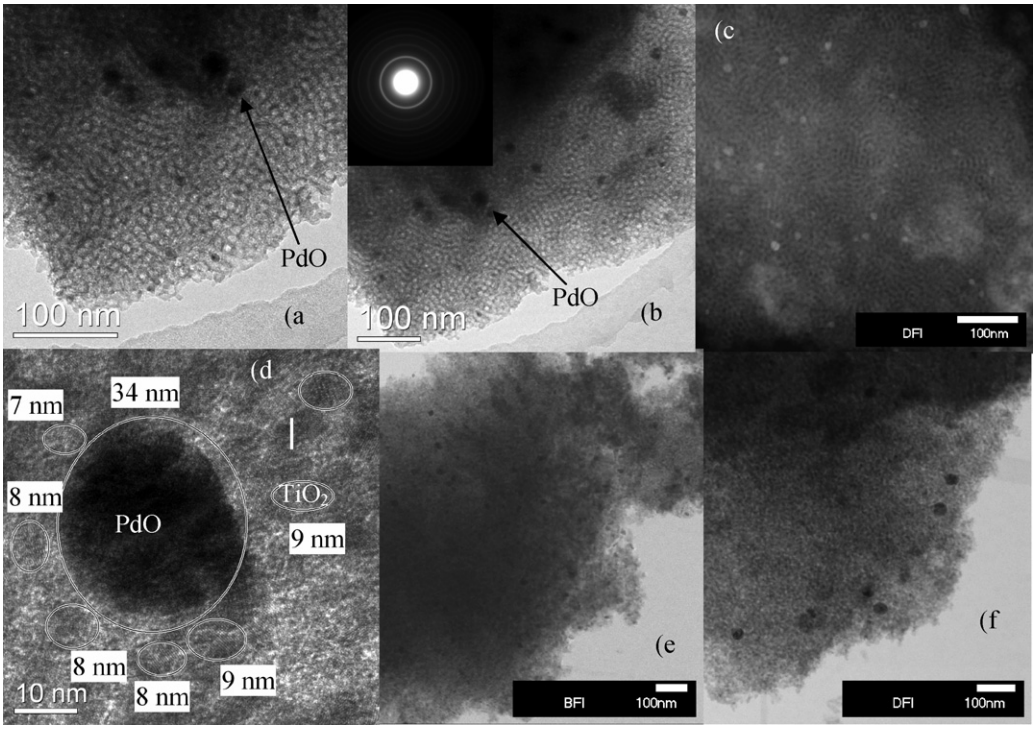

Fig. 4. TEM images of mesoporous 0.5 wt% PdO–TiO_2 nanocomposites calcined at 400 °C for 4 h (a), HRTEM image at 1 wt% PdO–TiO_2 (b) HRTEM image of 3 wt% PdO–TiO_2 showed PdO nanoparticles and TiO_2 anatase phase (d), the bright-field TEM images of 2 wt% PdO–TiO_2 (e) and the dark-field TEM image of PdO–TiO_2 at 1 (c) and 3 wt% (f).

PdO content in the composite materials is consistent with the Pd:Ti ratio used in the starting sol mixtures.

4. Photocatalytic activity

When photons with energies >3.2 eV, i.e., exceeding the band gap energy of TiO_2, are absorbed by the anatase particles in the mesoporous PdO–TiO_2 photocatalysts electrons are rapidly promoted from the valence band to the conduction band leaving holes behind in the valence band. The thus formed electrons and holes participate in redox processes at the semiconductor/water interface. It was considered that the changes in the valence states of Pd had an important effect on the behavior of photocatalytic oxidation of methanol over PdO–TiO_2. During the initial state of the reaction, photogenerated electrons were transferred from TiO_2 conduction band to the Pd^{2+} ions and Pd^{2+} ions have been reduced to Pd^0.

Also, our results showed that the color of PdO–TiO_2 (beige) nanocomposites were completely changed to black as a result of reduction of Pd^{2+} to Pd^0 through the photocatalytic reaction. The valance band holes migrate to the surface of the particles where they react with adsorbed hydroxide ions (or water molecules), generating adsorbed •OH radicals (Eqs. (1) and (2)), which are the key oxidants in the photocatalytic oxidation process [34]. At the same time, the conduction band electrons migrate through the three-dimensional TiO_2 network until they reach Pd^{2+} ions to reduce it to Pd^0 where adsorbed molecular O_2 is reduced to form $O_2^{\bullet-}$ radicals (Eqs. (3) and (4)). The α-hydroxy methyl radicals, formed from the reaction of the adsorbed •OH radicals with the adsorbed CH_3OH molecules can react with O_2 to form further HO_2• radicals [35] (Eqs. (5)–(7)). Obviously, the production of HCHO should be proportional to that of the •OH radicals, which plays a vital role in photocatalysis. Therefore, the photonic efficiency of HCHO can be used as an indicator of •OH production, and hence can be used to compare different photocatalysts [35]:

$$TiO_2 + h\nu \rightarrow TiO_2\,(e_{cb}^- + h_{vb}^+) \quad (1)$$

$$h_{vb}^+ + OH_s^- \rightarrow {}^\bullet OH_s \quad (2)$$

$$2TiO_2(e_{cb}^-) + Pd^{2+} \rightarrow 2TiO_2\text{–}Pd(e^-) \quad (3)$$

$$TiO_2\text{–}Pd(e^-) + O_2 \rightarrow TiO_2\text{–}Pd + O_2^{-\bullet} \quad (4)$$

$$CH_3OH + {}^\bullet OH_s \rightarrow {}^\bullet CH_2OH + H_2O \quad (5)$$

$${}^\bullet CH_2OH + TiO_2 \rightarrow HCHO + TiO_2(e^-) + H^+_{aq.} \quad (6)$$

$${}^\bullet CH_2OH + O_2 \rightarrow HCHO + HO_2{}^\bullet \quad (7)$$

According to the above mechanism, inhibiting the undesirable electron–hole pair recombination is important to enhance the photocatalytic activity because it can improve the ability to produce •OH radical group, which is possibly beneficial for oxidation of CH_3OH. The photocatalytic activities of all samples were evaluated for the photooxidation of CH_3OH to HCHO. The photonic efficiency (ζ) was calculated for each experiment as the ratio of the HCHO formation rate and the incident light intensity (Table 1). Fig. 5 shows the change of the HCHO concentration as a function of the irradiation time for the mesoporous PdO–TiO_2 nanocomposites at different PdO contents and Pd/Aeroxide TiO_2-P25. A linear relation of the HCHO concentration with irradiation time was obtained during the first 30 min of irradiation time. From this figure the HCHO formation rate was found to increase from 3.93×10^{-7} to 9.68×10^{-7} mol L^{-1} s^{-1} with increasing PdO content from 0 to 0.5 wt% and then decrease to 5.23×10^{-7} mol L^{-1} s^{-1} at 3 wt% PdO whereas the HCHO formation rates using TiO_2-P25 and Pd/TiO_2-P25 are 2.02×10^{-7} and 5.1×10^{-7} mol L^{-1} s^{-1} respectively. Apparently, the PdO and Pd nanoparticles serve as active sites for the electron transfer to O_2, on which the trapped photogenerated electrons are transferred to adsorbed molecular oxygen

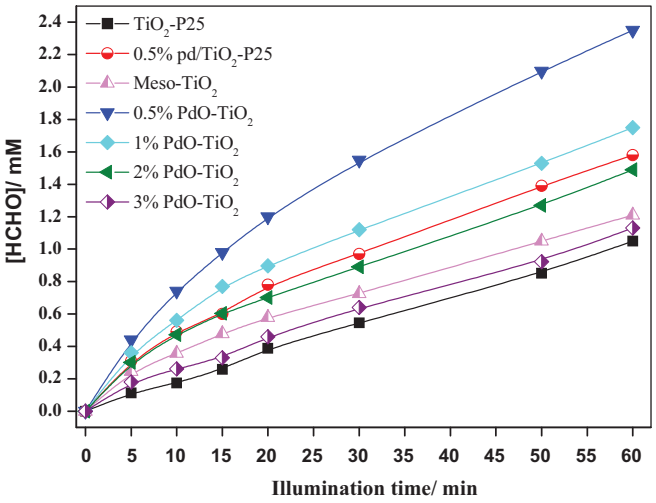

Fig. 5. HCHO formation as a function of illumination time over mesoporous PdO–TiO_2 nanocomposites at different PdO content 0, 0.5, 1, 2 and 3 wt% and commercial Aeroxide TiO_2-P25 and 0.5% Pd/TiO_2-P25. Photocatalyst loading, 0.5 g/L; 30 mM aqueous CH_3OH (O_2 saturated, natural pH; T = 20 °C); reaction volume, 75 mL; $I_o = 4.49 \times 10^{-6}$ Einstein L^{-1} s^{-1} (ca. >320 nm).

to produce $O_2^{\bullet-}$ radicals [14]. Fig. 6 and Table 1 show the photonic efficiencies of CH_3OH photooxidation using either PdO–TiO_2 nanocomposites or Pd/TiO_2-P25. The results reveal that the photonic efficiency increases with increasing PdO content up to 0.5% with the maximum photonic efficiency being 19.6%. Subsequently, the photonic efficiency gradually decreases with increasing PdO content reaching a value of 10.6% for the sample containing 3 wt% PdO. It is clearly seen that the mesoporous PdO–TiO_2 nanocomposites are more photoactive 4 and 2 times than the TiO_2-P25 and Pd/TiO_2-P25 (Table 1 and Fig. 6). In the presence of meso-TiO_2, the photonic efficiency of HCHO formation, ζ HCHO, is ca. 7.9% (Table 1). Such high photonic efficiencies of the mesoporous TiO_2 as compared with TiO_2-P25 can be attributed to several effects, such as a lower light scattering effect of the ordered mesopores, an accumulated local concentration of •OH [36], or a fast transport of the target molecule CH_3OH to the active sites due to the facile diffusion of the CH_3OH through the ordered porous network, which for the

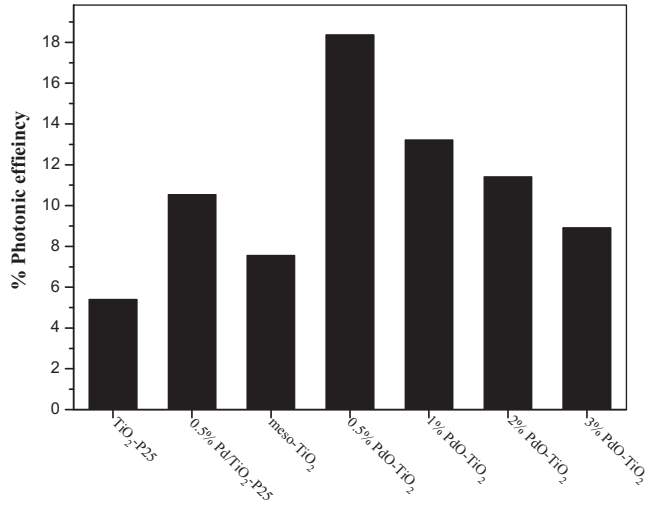

Fig. 6. Photooxidation of methanol to produce HCHO over mesoporous PdO–TiO_2 nanocomposites at different PdO content 0, 0.5, 1, 2 and 3 wt% and commercial Aeroxide TiO_2-P25 and 0.5% Pd/TiO_2-P25. Photocatalyst loading, 0.5 g/L; 30 mM aqueous CH_3OH (O_2 saturated, natural pH; T = 20 °C); reaction volume, 75 mL; $I_o = 4.49 \times 10^{-6}$ Einstein L^{-1} s^{-1} (ca. >320 nm).

TiO_2-P25 samples are hindered by the heterogeneities existing in the bulk sample. In addition, this difference can be explained by different surface areas, because the mesoporous TiO_2 is greater three times than TiO_2-P25 (Table 1). Since the larger surface area can offer more adsorption and reaction sites, the hierarchical porous TiO_2 network favors the diffusion of CH_3OH molecules to catalysis sites.

It is clearly seen that the addition of Pd is enhanced the photocatlatic activity of either TiO_2-P25 or meso-TiO_2. The purpose of loading TiO_2 with Pd is to generate at the interface between Pd and TiO_2 a Schottky barrier, which effectively captures the photogenerated electrons and reduces the rate of electron–hole recombination [37]. Therefore, noble metals can play a twofold role:(i) reduce the e^-/h^+ recombination as a consequence of the electron transfer from TiO_2 to noble metals and (ii) enhance the photoreduction efficiency owing to the Fermi level equilibration, thus ultimately leading to a higher yield of $^\bullet OH$. Assuming a Schottky contact between the mesoporous TiO_2 network and the noble metal particle, the Pd particles then serve as active sites for the reduction of molecular O_2, on which the trapped photogenerated electrons are transferred to O_2 producing $O_2^{\bullet-}$ radicals. It should be noted that it is frequently overseen that this latter process is really the "bottle-neck" in most photocatalytic transformations being the rate-determining step due to its very small thermodynamic driving force [14]. Thus its acceleration through the electron transfer catalysis induced by the Pd deposits will result in the observed increase in the photocatalytic activity of newly prepared photocatalysts.

To explain why 0.5 wt% PdO–TiO_2 nanocomposites is high photoactive? The interface being maximum at low PdO nanoparticles content and high dispersion, too large PdO particles (more than 0.5 wt%) could also act as recombination centers, detrimental to photocatalysis by hindering or avoiding the active photogenerated charge transfer to the reactant species at the surface [16,38,39]. Moreover, the presences of a large number of nanoparticles within the pore channels may also slow down mass transport and reduce the reaction rate. Therefore, the highest activity observed for the 0.5 wt% PdO–TiO_2 nanocomposites can be ascribed to the most efficient charge separation through the mesopore charge transfer [16,40,41]. The stability of the photocatalyst is also tested by cyclic performance. It is observed that the photonic efficiency of PdO–TiO_2 nanocomposites were slightly decreased at the first three cycles and it photonic efficiency is 18% and decreased to 15% at the fifth cycle, indicating that the photocatalysis activity of the composites is rather stable.

5. Conclusion

Preparation of highly active mesoporous PdO–TiO_2 nanocomposites with significantly improved photocatalytic activity has been achieved. The choice of the preparation procedure for mesoporous PdO–TiO_2 photocatalysts is shown to be of significant importance for the observed changes in their photocatalytic activity. The addition of PdO into the mesoporous TiO_2 network has been found to enhance the photocatalytic activity of TiO_2. The mesoporous PdO–TiO_2 nanocomposites are more photoactive 4 and 2 times than the commercially TiO_2-P25 and Pd/TiO_2-P25. PdO and Pd act as local electron reservoirs and prevent recombination of photogenerated holes and electrons upon the irradiation of UV light, although the predissolved oxygen also functions as an electron receiver in the reactions. Photocatalytic results indicate that these PdO–TiO_2 nanocomposites with mesopore structure enable high flux and rapid diffusion of methanol.

References

[1] C.T. Kresge, M.E. Leonowicz, W.J. Roth, J.C. Vartuli, J.S. Beck, Nature 359 (1992) 710.
[2] S.A. Davis, S.L. Burkett, N.H. Mendelson, S. Mann, Nature 385 (1997) 420.
[3] W.-S. Chae, S.-W. Lee, Y.-R. Kim, Chem. Mater. 17 (2005) 3072.
[4] A.A. Ismail, D.W. Bahnemann, J. Mater. Chem. 21 (2011) 11686–11707.
[5] A.A. Ismail, D.W. Bahnemann, ChemSusChem 3 (2010) 1057–1062.
[6] K. Nagaveni, G. Sivalingam, M.S. Hegde, G. Madras, Appl. Catal. B 48 (2004) 83.
[7] Y. Huang, W. Ho, S. Lee, L. Li, G. Zhang, J.C. Yu, Langmuir 24 (2008) 3510.
[8] H. Choi, M.G. Aantoniou, M. Pelaez, A.A. Delacruz, O.A. Shoemaker, D.D. Dionysiou, Environ. Sci. Technol. 41 (2007) 7530.
[9] J.C. Yu, J.G. Yu, W.K. Ho, Z.T. Jiang, L.Z. Zhang, Chem. Mater. 14 (2002) 3808.
[10] S. Tojo, T. Tachikawa, M. Fujitsuka, T. Majima, J. Phys. Chem. C 112 (2008) 14948.
[11] A.K. Sinha, K. Suzuki, J. Phys. Chem. B 109 (2005) 1708.
[12] (a) A.A. Ismail, Appl. Catal. B 85 (2008) 33–39;
(b) A.A. Ismail, Appl. Catal. B 58 (2005) 117–123.
[13] W.L. Kostedt, A.A. Ismail, D.W. Mazyck, Ind. Eng. Chem. Res. 47 (2008) 1483–1487.
[14] A.A. Ismail, D.W. Bahnemann, L. Robben, M. Wark, Chem. Mater. 22 (2010) 108.
[15] A.A. Ismail, D.W. Bahnemann, J. Phys. Chem. C 115 (2011) 5784–5791.
[16] (a) A.A. Ismail, D.W. Bahnemann, I. Bannat, M. Wark, J. Phys. Chem. C 113 (2009) 7429–7435;
(b) M. Alvaro, B. Cojocaru, A.A. Ismail, N. Petrea, B. Ferrer, F.A. Harraz, V.I. Parvulescu, H. Garcia, Appl. Catal. B: Environ. 99 (2010) 191–197.
[17] A.A. Ismail, D.W. Bahnemann, Green Chem. 13 (2011) 428–435.
[18] A.A. Ismail, Microporous Mesoporous Mater. 149 (2012) 69–75.
[19] F.H.B. Lima, J. Zhang, M.H. Shao, K. Sasaki, M.B. Vukmirovic, E.A. Ticianelli, R.R. Adzic, J. Phys. Chem. C 111 (2007) 404.
[20] L. Jiang, A. Hsu, D. Chu, R. Chen, J. Electrochem. Soc. 156 (2008) B370.
[21] J.W. Tang, H.D. Quan, J.H. Ye, Chem. Mater. 19 (2007) 116.
[22] D. Li, H. Haneda, S. Hishita, N. Ohashi, N.K. Labhsetwar, J. Fluorine Chem. 126 (2005) 69.
[23] Y.T. Kwon, K.Y. Song, W.I. Lee, G.J. Choi, Y.R. Do, J. Catal. 191 (2000) 192.
[24] V. Keller, P. Bernhardt, F. Grain, J. Catal. 215 (2003) 129.
[25] L. Cao, F.-J. Spiess, A. Huang, S.L. Suib, T.N. Obee, S.O. Hay, J.D. Freihaut, J. Phys. Chem. B 103 (1999) 2912.
[26] H. Yamashita, M. Honda, M. Harada, Y. Ichihashi, M. Anpo, T. Hirao, N. Itoh, N. Iwamoto, J. Phys. Chem. B 102 (1998) 10707.
[27] H. Li, Z. Bian, J. Zhu, Y. Huo, H. Li, Y. Lu, J. Am. Chem. Soc. 129 (2007) 4538–4539.
[28] S.J. Gregg, K.S.W. Sing, Adsorption, Surface Area and Porosity, Academic Press, London, 1982.
[29] T. Nash, Biochem. J. 55 (1953) 416.
[30] (a) N. Serpone, A. Salinaro, Pure Appl. Chem. 71 (1999) 303–320;
(b) A. Salinaro, A.V. Emeline, J. Zhao, H. Hidaka, V.K. Ryabchuk, N. Serpone, Pure Appl. Chem. 71 (1999) 321–335.
[31] C.G. Hatchard, C.A. Parker, A new sensitive chemical actinometer. II. Potassium ferrioxalate as a standard chemical actinometer, Proc. R. Soc. Ser. A 235 (1956) 518–536.
[32] S.J. Gregg, K.S.W. Sing, Adsorption. Surface Area and Porosity, Academic Press, London, 1997, pp. 111–194.
[33] R. Liu, Y. Ren, Y. Shi, F. Zhang, L. Zhang, B. Tu, D. Zhao, Chem. Mater. 20 (2008) 1140–1146.
[34] M.R. Hoffmann, S.T. Martin, W. Choi, D.W. Bahnemann, Chem. Rev. 95 (1995) 69–96.
[35] L. Sun, J.R. Bolton, J. Phys. Chem. 100 (1996) 4127.
[36] S. Tojo, T. Tachikawa, M. Fujitsuka, T. Majim, Chem. Phys. Lett. 384 (2004) 312–316.
[37] A.L. Linsebigler, G. Lu, J.T. Yates, Chem. Rev. 95 (1995) 735.
[38] S. Yin, H. Hasegawa, D. Maeda, M. Ishitsuka, T. Sato, J. Photochem. Photobiol. A: Chem. 163 (2004) 1.
[39] X.F. You, F. Chen, J.L. Zhang, M. Anpo, Catal. Lett. 102 (2005) 247.
[40] N. Lakshminarasimhan, E. Bae, W. Choi, J. Phys. Chem. C 111 (2007) 15244.
[41] Y. Huang, W. Ho, S. Lee, L. Zhang, G. Li, J.C. Yu, Langmuir 24 (2008) 3510.